

Holocene fire regimes across the Altai-Sayan Mountains and adjacent plains: interaction with climate and vegetation types

Dongliang Zhang^{1,2,3,*}, Blyakharchuk Tatiana⁴, Aizhi Sun^{5,*}, Xiaozhong Huang⁶, Yuejing Li^{1,2,3}

¹ State Key Laboratory of Ecological Safety and Sustainable Development in Arid Lands, Xinjiang Institute of Ecology and Geography, Chinese Academy of Sciences, 818 Beijing South Road, Urumqi, China.

² Research Center for Ecology and Environment of Central Asia, Chinese Academy of Sciences, 818 Beijing South Road, Urumqi, China.

³ University of Chinese Academy of Sciences, 19A Yuquan Road, Beijing, China.

⁴ Institute of Monitoring of Climatic and Ecological Systems, Siberian Branch of Russian Academy of Sciences, Tomsk, Russia.

⁵ College of Earth and Planetary Sciences, University of Chinese Academy of Sciences, Beijing, China.

⁶ College of Earth and Environmental Sciences, Lanzhou University, Lanzhou, China.

* Corresponding authors.

E-mail addresses: zhdl@ms.xjb.ac.cn (+86-18699198239) and aizhisun@ucas.ac.cn.

Abstract: The Altai-Sayan Mountains and adjacent plains (including the west Siberian Plain, Kazakhstan Hills and Junggar Basin) have experienced accelerated warming in recent decades, raising growing concerns about escalating wildfire risks. However, two key gaps hinder understanding: paleofire dynamics in western Mongolia are understudied and no comprehensive regional synthesis exists for charcoal influx across the Altai-Sayan ecoregion. To address this, we reconstructed the Holocene fire sequence in western Mongolia and analyzed the spatiotemporal variations in charcoal influx across different vegetation zones of the Altai-Sayan Mountains and adjacent plains, as well as their coupling relationships with vegetation structure. The results reveal that Holocene declines in charcoal influx were driven by distinct mechanisms across subregions: above the forest limit in the central Altai Mountains, the decline was primarily controlled by temperature-limited woody biomass availability; in the western Sayan Mountains, it stemmed from the substantial expansion of fire-resistant *P. sylvestris*. Since ~2 cal. kyr BP, intensified anthropogenic disturbances—specifically agricultural expansion and pastoral activities—have significantly increased fire frequency in the southeastern, western and northern Altai Mountains, the west Siberian Plain and the forest zones of central Altai Mountains. Conversely, the marked decline in charcoal influx observed in the

35 Khangai Mountains may be closely associated with vegetation fragmentation caused
36 by overgrazing. Our findings provide a long-term perspective on fire-vegetation-
37 climate interactions, offering critical insights for sustainable land management in the
38 Altai-Sayan ecoregion.

39 **Key words:** Charcoal influx; Fire activities; Vegetation; Altai-Sayan Mountains

40

41 **1. Introduction**

42 The North Europe-Siberia-Altai region is the core distribution area of boreal
43 forest ecosystems, hosting over 90% of the continent's boreal forest biomass and
44 terrestrial organic carbon stocks (Furyaev, 1996; Kasischke, 2000). Its dynamics are
45 closely intertwined with global climate system, forming a critical positive feedback
46 loop. In 2021, wildfires in the global boreal forests released 1.76 PgCO₂, setting a
47 historical record at that time (Zheng et al., 2023). Notably, the majority of carbon
48 emissions from boreal forests originated from northern Eurasia. Carbon sequestration
49 gain from a prolonged growing season may not offset carbon loss caused by enhanced
50 respiration and disturbances (Mo et al., 2023). This ecological transformation triggers
51 critical climate feedback mechanisms through carbon pool transformation, cascading
52 ecological and permafrost degradation (Ivanova et al., 2019; Jones et al., 2020). This
53 shift not only threatens regional carbon balance but also significantly accelerates
54 global warming by releasing massive amounts of greenhouse gases, underscoring the
55 extreme urgency of protecting this ecosystem for stabilizing the global climate.

56 Within this crucial northern Eurasian context, the Altai-Sayan region lies at the
57 junction of Arid Central Asia and the boreal forest ecosystems. This region features an
58 extremely steep hydrothermal gradient ranging from warm, arid steppes/shrublands in
59 the south to cold, humid closed-canopy boreal forests in the north, forming a vast and
60 sensitive ecotone (Xinjiang Comprehensive Investigation Team, CAS, 1978). It is
61 precisely this “marginal” and “transitional” nature that makes it a natural laboratory
62 and early warning system for studying fire-climate interactions (Fu et al., 2013; Liu et
63 al., 2021). The convergence of two key flammability drivers—coniferous vegetation
64 (*Pinus sibirica* dominance >60%) and intensifying drought regimes has created a

65 pyrogeographic hotspot. This synergy amplifies fire return intervals by $2.3\times$ compared
66 to pre-1990 baselines, fundamentally altering successional pathways and threatening
67 ecological security thresholds (Goldammer & Furyaev, 2013).

68 Remote sensing analyses document a quadrupling of fire events from 712 ± 89
69 yr^{-1} (1980-2000) to $3024\pm 214 \text{ yr}^{-1}$ (2001-2020) with burned area expanding
70 exponentially ($R^2=0.91$, $p<0.001$) (Ponomarev & Kharuk, 2016), which has a phase
71 coincidence with the dynamics of mean temperatures and climate dryness (Ponomarev
72 & Kharuk, 2016). In the southern Altai, the reduced burned area since 1987 can be
73 attributed to increased moisture and greatly increased investment in fire prevention
74 (Shi et al., 2021). The dynamic changes of fires in the instrumental measurement
75 period driven by human activities and natural processes exhibit distinct differences.
76 However, contemporary observations remain circumscribed by the temporal
77 resolution limitations of satellite archives (post-1980) and instrumental records,
78 creating a <50 -year observational window that inadequately captures decadal-scale
79 fire-climate-human feedbacks (Shi et al., 2021; Ponomarev & Kharuk, 2016; Albrich
80 et al., 2018; Kharuk et al., 2021). These both limit our understanding of long-term fire
81 activities in the ecological sensitivity regions.

82 Paleoecological approaches spanning centennial to millennial timescales provide
83 crucial temporal dimensional support for disentangling the complex interactions
84 through pattern-process analysis. Existing Holocene fire records in the Altai-Sayan
85 ecoregion have established a robust methodological framework for reconstructing
86 fire-vegetation-climate couplings (e.g., Blyakharchuk et al., 2004, 2007, 2008; Hu et
87 al., 2025; Li et al., 2024). However, two critical knowledge gaps remain to be
88 addressed: (1) the complete fire sequence in western Mongolia, and (2) the
89 spatiotemporal linkages between fire in this region and montane ecosystem dynamics
90 across the Altai-Sayan ecoregion. To address this issue, this study selected Achit Nuur
91 as the study site because of its continuous and stable depositional environment. Three
92 critical research dimensions include in this study: (1) Reconstructing fire variability in
93 the Holocene interval ($\sim 11.75-0$ cal. kyr BP) using high-resolution microscopic
94 charcoal analysis from Achit Nuur; (2) Identifying ecotonal heterogeneity in fire

95 regimes through comparison with other already-published paleofire records (n=23) in
96 the nearby regions; (3) Evaluating how dominant tree genera (*Abies*, *Betula*, *Larix*,
97 *Picea*, *P. sibirica*, *P. sylvestris*) and their summed percentages as forest cover
98 modulate fire characteristics across vegetation types. This study will clarify the
99 long-timescale fire history in the Altai-Sayan ecoregion, as well as its complex
100 associations with climate fluctuations, vegetation succession and human activities.
101 These outputs provide empirical foundations for developing climate-responsive fire
102 management strategies in the Central Asian ecosystems under the future scenarios.

103 **2. Physiographic Settings**

104 **2.1. The Altai-Sayan Mountains**

105 The Altai-Sayan Mountains, one of the most prominent mountain ranges in
106 Central Asia, connect with the Kazakhstan Hills to the west, border the Southern
107 Siberian Plain to the north, and adjoin the Junggar Basin-Khangai Mountains to the
108 south (Fig. 1; Feng et al., 2017). Climatologically, this region holds great significance,
109 as it likely served as a transitional zone where the Westerlies-dominated climates from
110 the west interacted with the Asian Monsoon-influenced climates from the east during
111 the Holocene (Blyakharchuk et al., 2004, 2008; Zhang & Zhang, 2025). Culturally, it
112 also functioned as a cultural crossroads between Asian and European civilizations
113 along the “Eurasian Steppe Silk Road” (Blyakharchuk & Chernova, 2013; Xiang et al.,
114 2023).

115 The North Atlantic Oscillation and Siberian High drive the southward
116 displacement of the Westerlies, which transport water vapor from the Mediterranean,
117 Caspian, and Black Seas into the study region during winter and spring (Aizen et al.,
118 2001; Kutzbach et al., 2014). In contrast, the interaction between the Asian Low and
119 Azores High regulates the northward shift of the Westerlies, facilitating water vapor
120 transport in summer and autumn (Aizen et al., 2001). These latitudinal shifts of the
121 westerlies induce a southward gradient of decreasing precipitation and increasing
122 climatic aridity, which in turn shapes the characteristic vegetation distribution patterns
123 across the Central Asia (Fig. 1). Zonally, vegetation distribution exhibits a strong
124 latitudinal dependence. Specifically, the coniferous forests dominate the southern

125 Siberian Plain, while the eastern Kazakhstan Hills and western Mongolia are
126 characterized by steppe ecosystems, and the Junggar Basin is covered by
127 desert-steppe (Chen, 2010). Additionally, the region's vegetation displays distinct
128 vertical zonation with communities transitioning from desert and steppe at lower
129 elevations to forest and alpine meadow at higher elevations (Blyakharchuk &
130 Chernova, 2013; Zhang et al., 2020).

131 **2.2. Achit Nuur**

132 Achit Nuur (49.42°N, 90.52°E; 1444 m a.s.l.) occupies an intermountain basin
133 bounded by the Mongolian Altai to the west, Mungen Taiga Mountain to the north and
134 Kharkhira Turgen Mountain to the east (site 1 in Fig. 1) (Sun et al., 2013). The lake
135 exhibits distinct shoreline zonation: low-lying northern/southern margins are
136 salt-marsh vegetation, while the elevated eastern and western shores are dominated by
137 desert steppe communities (Sun et al., 2013). Regional vegetation comprises a mosaic
138 of *Stipa krylovii*, *Stipa gobica* and *Cleistogenes soongorica* grasslands interspersed
139 with shrubs including *Artemisia frigida*, *A. xerophytica*, *A. caespitosa*, *Tanacetum*
140 *sibiricum*, *T. achillaeoides* and *T. trifidum*. Mountainous areas of the Mongolian Altai
141 host taiga forests dominated by *Larix sibirica* and *P. sibirica* with an understory of
142 *Rosa acicularis* and *Betula rotundifolia* (Sun et al., 2013).

143 A 2-m sediment core was retrieved from the central lake basin in 2010 using a
144 Livingston-type piston corer (Sun et al., 2013). Five lithological units were identified
145 based on organic matter (OM) content and mean grain size characteristics (Fig. 2A).
146 Ten bulk samples ([Table S1](#)) underwent accelerator mass spectrometry (AMS) ¹⁴C
147 dating at the University of Arizona NSF-AMS Facility (Fig. 2A). A 2100-year
148 reservoir correction was applied to all radiocarbon ages prior to calibration due to old
149 carbon-influenced 2099 ¹⁴C BP on the surface sediment and this correction is assumed
150 to be constant throughout the whole sequence (Sun et al., 2013). The calibration to
151 calendar years before present (cal. yr BP, relative to 1950 CE) utilized the IntCal20
152 curve (Reimer et al., 2020). The Bayesian age-depth model was reconstructed using
153 Bacon v2.5.3 (Blaauw & Christen, 2011) (Fig. 2B) **and median ages used to calculate**
154 **the sedimentation rates in yr/cm**. It should be pointed out that we analysed the

155 charcoal data in this study and the pollen and lithology were previously published
156 (Sun et al., 2013). This study just focused on the Holocene interval to investigate the
157 spatial heterogeneities of fire regimes in the Altai-Sayan Mountains and adjacent
158 plains.

159 **2.3. Other study sites in the Altai-Sayan Mountains and adjacent plains**

160 A total of 24 sites, including Achit Nuur (Table 1), were selected to investigate
161 the spatial heterogeneity in fire regimes across the Altai-Sayan Mountains and
162 adjacent plains. These sites were divided into seven regions based on the vegetation
163 distribution and geographic location.

164 Southeastern/western Altai Mountains within steppe zone (Region A, n=4):
165 Tolbo Lake (site 2; 48.55°N, 90.05°E, 2080 m a.s.l.) is an alpine lake of glacial origin
166 covered by mountain steppe in the Mongolian Altai (Hu et al., 2024). Alahake Lake
167 (site 3; 47.69°N, 87.54°E, 483 m a.s.l.) is located in the Irtysh River valley in the
168 southern Altai Mountains (Li et al., 2019). Kuchuk Lake (site 4; 52.69°N, 79.84°E, 98
169 m a.s.l.) is the largest endorheic basin in Kulunda Basin within the southern Siberia
170 (Rudaya et al., 2020).

171 Low-relief west Siberian plain (Region B, n=4): Rybnaya Mire (site 5; 57.28°N,
172 84.49°E) is located near the Rybnaya River in the southern taiga of Western Siberia
173 (Feurdean et al., 2022). Plotnikovo Mire (site 6; 56.88°N, 83.30°E, 120 m a.s.l.) is an
174 ombrotrophic bog located at the eastern margins of the Great Vasyugan Mire in
175 Western Siberia (Feurdean et al., 2020). Shchuchye Lake (site 7; 57.13°N, 84.61°E, 80
176 m a. s. l.) is located in the south taiga zone of the West Siberian plain (Blyakharchuk
177 et al., 2024). Ulukh–Chayakh Mire (site 8; 57.34°N, 88.32°E) is located on a terrace
178 of the Chulym river in the southern taiga of Western Siberia (Feurdean et al., 2022).

179 Northern Altai Mountains (Region C, n=4): Chudnoye Lake (site 9; 54.03°N,
180 89.01°E, 1147 m a.s.l.), Tundra Mire (site 10; 53.79°N, 88.27°E, 247 m a.s.l.) and
181 Kuatang Mire (site 12; 51.81°N, 87.32°E, 650 m a.s.l.) are located in the northern
182 Altai Mountains in areas covered by wet mountain dark coniferous (with *Abies*, *P.*
183 *sibirica* and *Betula*) taiga (Blyakharchuk & Pupysheva, 2022; Blyakharchuk et al.,
184 2024). Mokhovoe Bog (site 11; 52.52°N, 86.42°E, 283 m a.s.l.) is located on the

185 western piedmont of north Altai covered by birch (with *B. pendula*+*B. pubescens*)
186 and pine (*P. sylvestris*) forest-steppe (Blyakharchuk & Pupysheva, 2022).

187 Central Altai Mountains within the forest zone (Region D, n=3): Dzhangyskol
188 Lake (site 13; 50.18°N, 87.73°E, 1800 m a.s.l.) is situated in the western Kurai
189 intermontane depression covered with steppe vegetation and bounded by small hills
190 with *P. sibirica* and *L. sibirica* (Blyakharchuk et al., 2008). Two freshwater lakes are
191 situated 1.5-4 km apart at different elevations below the timberline in the Ulagan
192 Plateau: Uzunkol Lake (site 14; 50.48°N, 87.1°E, 1985 m a.s.l.) and Kendegelukol
193 Lake (site 15; 50.50°N, 87.63°E, 2050 m a.s.l.) (Blyakharchuk et al., 2004).

194 Central Altai Mountains above the forest limit (Region E, n=3): Tashkol Lake
195 (site 16; 50.45°N, 87.67°E, 2150 m a.s.l.) lies at the timberline (upper limit of
196 continuous forest) of Ulagan Plateau in the central part of Russian Altai
197 (Blyakharchuk et al., 2004). Akkol Lake (site 17; 50.25°N 89.62°E, 2204 m a.s.l.) and
198 Grusha Lake (site 18; 50.38°N, 89.42°E, 2413 m a.s.l.) are situated in the western
199 Kargininskaya high-mountain depression near the junction of the Chikhachev and
200 Shapshal ranges of the south-eastern part of Russian Altai (Blyakharchuk et al., 2007).

201 Western Sayan Mountains (2000-2700 m a.s.l.) (Region F, n=3): Buibinskoye
202 Mire (site 19; 52.84°N, 93.52°E, 1377 m a.s.l.) and Bezrybnoye Mire (site 20;
203 52.81°N, 93.50°E, 1395 m a.s.l.) are located in the Yergaki Nature Reserve
204 (Blyakharchuk, 2020). Lugovoe Mire (site 21; 52.85°N, 93.35°E, 1299 m a.s.l.) is the
205 largest mire in the Yergaki Natural Park with the largest hydrological catchment in the
206 Western Sayan Mountains (Blyakharchuk and Chernova, 2013).

207 Khangai Mountains (peaks 4031 m a.s.l.) (Region G, n=3): Three selected sites
208 include Olgi Lake (site 22; 48.32°N, 98.01°E, 2012 m a.s.l.) (Unkelbach et al., 2021),
209 Shireet Naiman Nuur (site 23; 46.53°N, 101.82°E, 2429 m a.s.l.) (Barhoumi et al.,
210 2024) and Ugii Nuur (site 24; 47.77°N, 102.78°E, 1330 m a.s.l.) (Wang et al., 2011).

211 **3. Methods**

212 **3.1. Charcoal analysis**

213 The pre-treatment process for charcoal analyses involved the standard pollen
214 extraction method (Tang et al., 2022; Wang et al., 2024). Charcoal particles were

215 identified using a light microscope, characterized by dark black color, opaque
216 appearance, sharp corners, and straight edges. The treated samples were prepared into
217 pollen slides by adding an appropriate amount of glycerin using the particle counting
218 method, which were then observed and counted under a Lycra microscope. A total of
219 more than 300 particles of all sizes were quantified at 400× magnification using an
220 Olympus BX53 microscope and the quantity of Lycopodium spores was determined
221 for each sample.

222 The concentration of charcoal was then calculated based on the statistical data
223 (Li et al., 2024):

$$W = A * N / (n * N)$$

224 Where W is the charcoal concentration (particles/g), A is the the total count of
225 charcoal fragments, n is the number of additional lycopodium spores per mount, N is
226 the statistical number of lycopodium spores, and G is the sample weight (g). Charcoal
227 influx (CHAR, particles/cm²/yr) is calculated by multiplying the concentration
228 dividing by the sedimentation rate (yr/cm) derived from the age-depth model (see
229 paragraph 2.2).

230 3.2. Generalized additive models

231 Generalized additive models (GAMs) employ a link function to examine the
232 relationship between the mean of the response variable (i.e., dependent variable) and a
233 smoothed function of the predictor variable (i.e., independent variable). The model
234 convergence and adequacy were assessed using the gam.check() function in R and
235 confirmed that the basis dimensions (k) were sufficient and inspected diagnostic plots
236 of residuals to ensure the model structure was appropriate. In this study, we
237 investigated the associations between charcoal influx and two types of predictors: (1)
238 individual taxa, including *Abies*, *Betula*, *Larix*, *Picea*, *P. sibirica* and *P. sylvestris*,
239 because they represent the dominant arboreal species in the study area and are key
240 components of the regional forest ecosystems; and (2) total forest cover, defined as
241 the summed percentage of the aforementioned six taxa.

242 We constructed GAMs with a quasi-Poisson distribution and a log link function
243 using the mgcv package in R (Wood, 2017). This distribution was selected because it

244 flexibly corrects for overdispersion without requiring a specific parametric
 245 distribution for the data (Wood, 2017). For all smoothing terms, we used thin-plate
 246 splines as the basis function—this is the default setting in the `gam()` function of the
 247 `mgcv` package. The model fitting was performed via restricted maximum likelihood
 248 (REML) for smoothness selection.

249 **3.3. Data processing for comparison**

250 To render charcoal influx records from different sites comparable, a three-step
 251 transformation procedure was applied to calculate comparable Z-scores (Power et al.,
 252 2007):

253 (1) Min-max transformation: Raw influx values were rescaled to a 0-1 range to
 254 reduce the influence of varying magnitudes between sites.

$$255 \quad C'_i = (C_i - C_{min}) / (C_{max} - C_{min})$$

256 In this expression, C'_i is the value of mini-max transformed for the i -th sample at
 257 each sequence, C_i is the charcoal influx (CHAR) value for the i -th sample at each
 258 sequence, C_{max} is the maximum value of C_i , and C_{min} is the minimum value of C_i .

259 (2) Box-Cox transformation for homogenization of variance: This
 260 transformation was applied to homogenize within-record variance and improve the
 261 normality of the data distribution, satisfying the assumptions for subsequent statistical
 262 analyses.

$$C_i^* = \begin{cases} ((C'_i + \alpha)^\lambda - 1) / \lambda, & \lambda \neq 0 \\ \log(C'_i + \alpha), & \lambda = 0 \end{cases}$$

263 In this expression, C_i^* is the Box-Cox value transformed for C'_i , λ is the
 264 parameter of Box-Cox transformation estimated using maximum likelihood, and α is a
 265 small constant added to ensure all data values are positive (>0) prior to the Box-Cox
 266 transformation, as the function cannot handle zero values.

267 (3) Z-score calculation: The transformed data were converted into Z-scores
 268 (standardized anomalies with a mean of 0 and unit variance) to facilitate direct
 269 comparison and the synthesis of charcoal records across different sites.

$$Z - \text{score} = (C_i^* - \overline{C_i^*}) / \delta$$

270 In this expression, $\overline{C_i^*}$ is the average value of C_i^* and δ is the standard deviation

271 of C_i^* .

272 Considering the ~200-year sample resolution at most sites, the transformed
273 Z-scores were linearly interpolated to 200-year time steps. Subsequently, the
274 interpolated data were averaged using a binning method to construct composite curves
275 that characterize fire regimes across different regions. The Holocene interval was
276 divided into three intervals: early Holocene (~11.75~8.2 cal. kyr BP), middle
277 Holocene (~8.2~4.2 cal. kyr BP) and late Holocene (~4.2~0 cal. kyr BP) (Marcott et
278 al., 2013).

279 4. Results and Discussions

280 4.1. Reconstructed fire history and its relationship with vegetation at Achit Nuur

281 The charcoal influx in Achit Nuur varies from 67 to 2643 particles/cm²/yr with an
282 average of 501 particles/cm²/yr. Notably, higher charcoal influx has been recorded
283 since ~2 cal. kyr BP with the maximum occurring during the interval of ~1.2~0.79
284 cal. kyr BP (Fig. 3a). Regarding pollen trends: *P. sibirica*, *Betula* and *Picea* exhibited
285 a rapid increase before ~6 cal. kyr BP, followed by a gradual decreasing trend (Fig. 3b)
286 (Sun et al., 2013). High *Larix* pollen content was observed from ~6 to ~2 cal. kyr BP,
287 while *Abies* pollen remained relatively low throughout the entire sequence. GAMs
288 analyses reveal charcoal influx is significantly positively correlated with the
289 abundance of *Betula* (Deviance explained=20%, p=0.02), *P. sibirica* (Deviance
290 explained=34.5%, p=0.001) and total forest cover (Deviance explained=41.5%,
291 p<0.001). Conversely, it is significantly negatively correlated with decreasing *Larix*
292 (Deviance explained=41.9%, p<0.001) and *Picea* (Deviance explained=19.2%,
293 p=0.001) abundances (Table 2, Fig. 1).

294 The strong positive relationship between charcoal and forest cover suggests that
295 this region functions as a fuel-limited system, where biomass availability regulates
296 fire activities. Mechanistically, the late-Holocene fire increase coincides with a shift
297 in vegetation composition: the decline of *Larix* (often a fire-avoidant species that
298 maintains moister sub-canopy conditions) after ~2 cal. kyr BP likely increased
299 landscape flammability. In contrast, taxa such as *Betula* and *P. sibirica* possess traits
300 like thinner bark and more resinous tissues (Feurdean et al., 2020, 2022) that facilitate

301 fire spread and intensity. Thus, these shifts in relative species directly regulated the
302 observed variation in charcoal influx.

303 **4.2. Holocene climate-fuel feedbacks across selected sites**

304 **4.2.1. Southeastern/western Altai Mountains within the steppe zone (Region A):**

305 Charcoal records from four lacustrine systems (Achit Nuur, Tolbo, Alahake and
306 Kuchuk Lakes) reveal a consistent amplification of fire activity during the late-
307 Holocene (Fig. 4b). Distinct peak intervals vary across sites: ~1.2-~0.79 cal. kyr BP at
308 Achit Nuur, ~1.20-~0.65 cal. kyr BP at Tolbo Lake, ~1.44-~1.02 cal. kyr BP at
309 Alahake Lake, and a pronounced doubling of charcoal flux over the past two
310 millennia at Kuchuk Lake. Pollen spectra highlight the ecosystem-specific fuel
311 configurations that underpin these fire patterns: Tolbo Lake is dominated by an alpine
312 steppe ecosystem (*Artemisia*-*Poaceae*), where herbaceous plants serve as the primary
313 surface fuel; Achit Nuur features montane *P. sibirica* providing highly flammable
314 resinous fuel sources. Alahake Lake is surrounded by lowland *Picea-Larix* mixed
315 forest, where leaf litter and understory vegetation contribute to fuel loads (Sun et al.,
316 2013; Hu et al., 2024; Li et al., 2019; Rudaya et al., 2020).

317 This divergence in fuel strategy explains the varied fire responses to
318 environmental changes. GAMs analyses confirm that charcoal influx at Achit Nuur
319 and Tolbo Lake is primarily controlled by forest cover (Table 2, Fig. S1). Specifically,
320 *Larix* (41.9% deviance explained) and *P. sibirica* (34.5%) are key drivers in Achit
321 Nuur, whereas *P. sibirica* (13.3%) plays a dominant role at Tolbo Lake. At Alahake
322 Lake, *Betula* (with its thin bark and volatile leaf litter) is the primary combustion
323 source. Notably, at Kuchuk Lake, the post-2 cal. kyr BP doubling of charcoal influx is
324 explicitly linked to the expansion of *Betula* and *P. sylvestris* forest—both of which
325 possess high ignition potential (Table 2, Fig. S2).

326 **4.2.2. West Siberian plain (Region B, n=4):**

327 Rybnaya Mire, located on the low terrace of the Ob' River (83 m a.s.l.) and
328 dominated by *P. sylvestris* and *Betula*, shows higher influx during the middle
329 Holocene but no significant charcoal pulse over the past 50 years (Feurdean et al.,
330 2020) (Fig. 4c). GAM analysis indicates fire activity is primarily controlled by

331 coniferous vegetation with *Picea* abundance explaining 44.5% of the variance (Table
332 2, Fig. S2). In contrast, Plotnikovo Mire exhibits a rapid charcoal increase since ~2
333 cal. kyr BP (Feurdean et al., 2020). This surge is likely linked to the gradual
334 expansion of *Betula* (forest cover explaining 39.7% of deviance) (Table 2, Fig. S2), as
335 the accumulation of its flammable resinous bark created more favorable conditions for
336 fire ignition and spread (Feurdean et al., 2022). Shchuchye Lake displays a phased
337 fire regime, marked by a strong charcoal pulse at the Younger Dryas-Early Holocene
338 transition (~12~11 cal. kyr BP) and slightly increased fire activity during the late
339 Holocene (Fig. 4c). Ulukh-Chayakh Mire records key fire events in the last
340 millennium and during the ~4.5~3 cal. kyr BP interval (Fig. 4c).

341 GAM analyses reveal the divergent fire-vegetation relationships rooted in
342 canopy structure (Table 2, Fig. S2 and S3): (1) Negative correlation at Rybnaya and
343 Plotnikovo Mires (canopy cover >75%): Dense canopies limit light availability,
344 maintaining humid microclimatic that suppress the herbaceous understory growth.
345 This creates moist surface conditions and sparse fine fuels, resulting in an inverse
346 relationship between canopy cover and fire. (2) Positive correlation at Shchuchye
347 Lake (canopy cover <65%): Open canopy structures allow solar radiation to reach the
348 forest floor, promoting the growth of flammable grassy understories. These fine fuels
349 dry quickly and ignite easily, while the open environment facilitates air circulation
350 and fire spread, leading to a positive association between canopy openness and
351 charcoal influx.

352 **4.2.3. Northern Altai Mountains (Region C, n=4):**

353 Chudnoye Mire, situated in a remote mountain taiga near the upper forest limit
354 (Fig. 1), exhibits a decline in influx during the early to mid-Holocene followed by
355 late Holocene intensification (Fig. 4d). This variations correlates positively with
356 *Betula* (30.3%) and *Picea* (20.5%) abundances (Table 2, Fig. S3). The mechanism lies
357 in pyrophytic properties of these taxa (*Betula* and *Picea*): their needle litter and
358 resinous tissues that are highly flammable when dry, directly boosting fire frequency
359 (Blyakharchuk et al., 2024).

360 Tundra Mire, characterized by dense forests of *Abies* and *Betula*, shows rising

361 charcoal influx after ~4 cal. kyr BP. GAM analysis suggests that this trend stems from
362 the fire-adapted traits of *Larix* (22.7% of deviance explained) (Table 2, Fig. S4).
363 Mokhovoe Bog, a birch forest-steppe site, records four charcoal influx peaks at
364 ~11.5~9.5, ~8.5~7, ~5.6~4 and ~1.5~1 cal. kyr BP. A statistical correlation
365 (11.9%) with *Picea* pollen (Table 2, Fig. S4) suggests a climatic controls on fuel
366 production: humid conditions enhance bioproductivity and litter accumulation.
367 Although *Picea* is less flammable than *Betula*, the sheer increase in fuel loads drives
368 higher charcoal influx (Blyakharchuk, 2022).

369 Kuatang Lake shows a clear charcoal increase between ~3.5 and ~2 cal. kyr BP
370 (Fig. 4d, Fig. S4). A distinct vegetation-fire pattern emerges here: charcoal influx
371 positively correlated with *Betula* pollen but negatively with *Abies*, *P. sibirica* and *P.*
372 *sylvestris*. This suggests that the post-3.5 cal. kyr BP fire increase was driven by the
373 expansion of fire-prone *Betula* (thin, volatile bark) at the expense of more fire-
374 resistant conifers (thick bark, dense canopies) (Blyakharchuk et al., 2024).

375 **4.2.4. Central Altai Mountains within the forest zone (Region D, n=3):**

376 Charcoal influx exhibited a consistent increasing trend across Kendegelukol
377 Lake, Uzunkol Lake and Dzhangyskol Lake (Fig. 4e), with pronounced acceleration
378 during the late Holocene. Uzunkol Lake records a sharp rise in charcoal influx since
379 ~1.2 cal. kyr BP, while Dzhangyskol Lake increases markedly from ~0.5 cal. kyr BP
380 onward. Notably, Uzunkol Lake also documented elevated charcoal influx between
381 ~9.5 and ~9 cal. kyr BP, coinciding with the steppe-to-forest transition
382 (Blyakharchuk et al., 2008). This early Holocene peak likely arose from an unstable
383 fire regime during the forest establishment: dry climatic conditions combined with
384 increasing woody fuel loads made the nascent ecosystem highly susceptible to
385 ignition (Blyakharchuk & Pupysheva, 2022). The subsequent landscape stabilization
386 and humidification suppressed fire activity until the late Holocene (Zhang and Zhang,
387 2025).

388 Kendegelukol Lake and Dzhangyskol Lake exhibited modest increases in
389 charcoal influx throughout the Holocene (Fig. 4e). This contrast highlights Uzunkol
390 Lake's sensitivity as an ecotone site (Blyakharchuk et al., 2004). Located in the

391 forest-steppe transition zone, its dynamic vegetation mix is highly responsive to minor
392 climatic fluctuations, amplifying fire signals. In contrast, the cohesive forests at these
393 two sites buffer against small-scale environmental changes (Lezine et al., 2023).
394 GAM analyses across all three lakes reveal strong positive correlations with *Abies*,
395 *Betula* and *P. sylvestris* (Table 2, Fig. S5), confirming that late-Holocene forest
396 expansion enhanced fuel accumulation, thereby lowering ignition thresholds.

397 **4.2.5. Central Altai Mountains above the forest limit (Region E, n=3):**

398 Tashkol Lake (2150 m a.s.l.) exhibits a sharp peak in charcoal influx at ~11–10.5
399 cal. kyr BP, likely caused by a paraglacial mechanism: meltwaters redeposition of
400 Pleistocene-aged microcharcoal following deglaciation (Blyakharchuk et al., 2004,
401 2024). Subsequently, the middle Holocene warming (~10.5–4 cal. kyr BP) promoted
402 high-elevation expansion, increasing biomass and charcoal influx via a temperature-
403 dependent mechanism. Late Holocene cooling reversed this trend.

404 Grusha Lake (2413 m a.s.l.) shows a similar pattern with an exceptionally late-
405 glacial (~12–11 cal. kyr BP) high charcoal influx attributed to the allochthonous
406 redeposition (Rudoy and Yatsuk, 1986; Blyakharchuk et al., 2024). Following
407 deglaciation (~10.5 cal. kyr BP), vegetation colonization stabilized the landscape,
408 shifting the record to reflect in-situ fire activity (Blyakharchuk et al., 2004). Akkol
409 Lake mirrors the general trend but lacks the ~12–11 cal. kyr BP peak. This absence is
410 explained by its lower elevation and lack of glacial coverage during the last glaciation
411 (Blyakharchuk et al., 2007). Without glaciers to accumulate ancient microcharcoal,
412 and with drier conditions inhibiting sediment transport, Akkol Lake records only
413 minimal in-situ fire activity during this period.

414 GAMs analyses identify the key vegetation sources of biomass combustion
415 across three lakes: *Picea* (40.7%) in Tashkol Lake; a combination of *Picea* (31.6%)
416 and *Larix* (30.4%) in Akkol Lake; and *Larix* (49.3%) and *Picea* (35.80%) in Grusha
417 Lake (Table 2, Fig. S6). These species-specific associations reflect differences in fuel
418 flammability — *Larix* produce resin-rich needles and bark that ignite easily, while
419 *Picea* litter, though less flammable, contributes to fuel loads when accumulated in

420 large quantities (Blyakharchuk et al., 2004) — ultimately driving lake-specific
421 variations in charcoal influx. Notably, significant differences in charcoal influx
422 magnitudes and timing were observed among three lakes, largely tied to their distinct
423 elevations, glacial histories and post-glacial vegetation development.

424 **4.2.6. Western Sayan Mountains (Region F, n=3):**

425 Records from Lugovoe Peat, Bezrybnoye Mire and Buibinskoye Mire generally
426 show decreasing Holocene charcoal records. A notable exception is the ~12-~11 cal.
427 kyr BP peak at Buibinskoye Mire (Fig. 4g). As permafrost receded and the region
428 transitioned from cold, waterlogged soils supporting sparse *Picea* to better-drained
429 substrates, *P. sibirica* and *Abies* expanded (Blyakharchuk et al., 2013, 2022). The ~11
430 cal. kyr BP peak reflects this forestation event. A transient warming just prior
431 (~11.5-~11 cal. kyr BP) likely dried sparse spruce litter, triggering intense fires.
432 Following a mid-Holocene maximum (~10.5-~7 cal. kyr BP) driven by warming-
433 enhanced productivity, charcoal influx declined as late-Holocene cooling reduced fuel
434 accumulation.

435 GAMs results highlight species-specific roles in driving charcoal influx: in
436 Lugovoe Peat, *Abies* and *Larix* are the primary contributor to charcoal production.
437 However, at Bezrybnoye Mire, fire-resistant *P. sylvestris* explains the most variance
438 (28.10%) (Table 2, Fig. S7). This suggests a negative feedback: the expansion of *P.*
439 *sylvestris* displaced more flammable taxa, reducing overall forest flammability and
440 driving the long-term decline in charcoal influx.

441 **4.2.7. Khangai Mountains (Region G, n=3):**

442 At Olgi Lake, a negative correlation (33.3%) between charcoal influx and
443 primary forest cover suggests fires are fueled by steppe herbs (Table 2, Fig. S8). An
444 decrease in forest cover would promote grass-fueled fires, leading to higher charcoal
445 influx—explaining the observed negative correlation (Sun et al., 2013). Conversely, at
446 Shireet Naiman Nuur (37.4%) and Ugii Nuur (18.4%), positive correlations with
447 forest cover (especially *P. sibirica*) (Table 2, Fig. S8) indicate woody biomass drives
448 fire activity. Despite similar trends, Shireet Naiman Nuur records lower overall influx
449 due to elevation-limited productivity (Barhoumi et al., 2024).

450 Marked charcoal spikes were recorded at Olgi Lake (~3.4~3.1 cal. kyr BP)
451 and Ugii Nuur (~2.4~2.1 cal. kyr BP), which align with periods of local drought
452 (Unkelbach et al., 2021; Barhoumi et al., 2024; Wang and Feng, 2013). In the absence
453 of significant human impact during these intervals, drought likely acted as a natural
454 catalyst, drying fuels and increasing susceptibility to ignition.

455 **4.3. Holocene climate-fuel feedbacks across the different regions**

456 In Region A, fire activity was suppressed during the dry early Holocene due to
457 limited fuel availability (Zhang and Zhang, 2025; Sun et al., 2013; Hu et al., 2024; Li
458 et al., 2021; Rudaya et al., 2020). From the mid-Holocene to ~2 cal. kyr BP, increased
459 precipitation (Hu et al., 2024; Zhang and Zhang, 2025) facilitated vegetation
460 expansion, fueling a gradual rise in fires. Crucially, after ~2 cal kyr BP, anomalous
461 charcoal peaks across all sites correlate with pollen evidence of agricultural expansion
462 (e.g., cereal-type Poaceae; Xiao et al., 2021). This synchrony suggests that
463 anthropogenic disturbances — specifically intentional burning for pasture and crop
464 management — overrode climatic controls to become the dominant driver of fire
465 frequency (Li et al., 2021; Xiao et al., 2021; Rudaya et al., 2020).

466 In Region B, fire history divides into three phases: (1) An early pulse (~12~11
467 cal. kyr BP) at Shchuchye Lake driven by paraglacial processes (Blyakharchuk et al.,
468 2024); (2) A mid-Holocene increase (~8.5~6 cal. kyr BP) at Rybnaya Peat linked to
469 the expansion of dark taiga (Feurdean et al., 2022); and (3) A widespread fire surge
470 past ~2 cal. kyr BP. This late-Holocene intensification resulted from the synergistic
471 effects of megadrought conditions (drying vegetation) and the emergence of
472 pastoralist fire use (Feurdean et al., 2022).

473 In Region C, a late-Holocene increase in fire activity (following an early-
474 Holocene decline) correlates with regional humidification and intensified human
475 occupation (Blyakharchuk et al., 2023; Zhang and Zhang, 2025). While moisture
476 increased biomass, human activities provided ignition sources. Notably, charcoal
477 pulses in the Bronze Age (~4~3 cal. kyr BP) and Early Iron Age (~3 cal. kyr BP)
478 coincide with metallurgical centers in the Kuznetski Alatau (Slavnin and Sherstova,

479 1999), linking fire history directly to cultural expansion (Panyushkina, 2012; Agatova
480 et al., 2014; Xiang et al., 2024; Blyakharchuk, 2022; Slavnin and Sherstova, 1999).

481 In Region D, a 2.3-fold increase in charcoal influx over the last two millennia
482 (Fig. 4e) reflects the cumulative impact of forest expansion (natural fuel buildup) and
483 pastoral burning. The sharp rise after ~1.0 cal kyr BP, in particular, points to
484 intensified land clearance and management by pastoralists, which altered vegetation
485 structure and amplified flammability (Zhang et al., 2022; Blyakharchuk et al., 2004,
486 2008).

487 In Regions E and F, long-term trends differ mainly by vegetation trajectory. In
488 Region E, temperature-driven (Blyakharchuk et al., 2007) forest fluctuations dictated
489 fuel loads (Fig. 4f), with a late anthropogenic overprint. In Region F, the progressive
490 expansion of fire-resistant *P. sylvestris* caused a long-term reduction in ecosystem
491 flammability, driving a decline in charcoal influx despite climatic changes
492 (Blyakharchuk et al., 2013, 2022).

493 In Region G, a disconnect emerges in the late Holocene: despite a humid climate
494 that should support biomass, charcoal influx declined (Unkelbach et al., 2021;
495 Barhoumi et al., 2024). This anomaly is attributed to anthropogenic landscape
496 fragmentation caused by intense grazing (Zhang S.J. et al., 2021). As observed in
497 modern studies, livestock remove fine surface fuels, effectively severing fuel
498 connectivity and suppressing fire spread (Umbanhowar et al., 2009).

499 Broadly, Holocene fire regimes in the Altai-Sayan Mountains and adjacent plains
500 reflect a shift from climate-limited systems to human-modified systems. Before ~2 cal.
501 kyr BP, fire activity was largely regulated by moisture (limiting fuel in steppe regions
502 A & G) or temperature (limiting fuel in alpine/forest regions E & F). Since ~2 cal. kyr
503 BP, a divergence occurs: in regions with expanding agriculture/pastoralism (A, B, C,
504 D), anthropogenic ignition sources amplified fire activity beyond natural baselines.
505 Conversely, in heavily grazed areas (Region G), pastoral pressure fragmented fuels,
506 suppressing fires. This synthesis highlights the fundamental transition of the Altai-
507 Sayan fire regime from biophysical control to anthropogenic dominance in the late
508 Holocene.

509 **5. Conclusions**

510 This study presents a long-term fire record from western Mongolia and
511 systematically evaluates the spatiotemporal variations in charcoal influx and its
512 coupling with vegetation across the Altai-Sayan Mountains and adjacent plains. Our
513 synthesis reveals distinct regional drivers of fire regimes rooted in climate-fuel
514 feedbacks and, more recently, anthropogenic forcing:

515 Prior to ~2 cal. kyr BP: Fire activity was primarily regulated by biophysical
516 constraints on fuel availability. In the steppe zone (Region A), low charcoal influx
517 was driven by aridity, which limited vegetation productivity and fuel continuity. In the
518 Central Altai forests (Regions D and E) and Western Sayan (Region F), fire trends
519 generally followed temperature-regulated forest dynamics. Specifically, the early-to-
520 mid Holocene decline in charcoal influx (Regions D, E, and F) reflected shifts in
521 forest composition and cover. Notably, in Region F, this decline was mechanistically
522 linked to the expansion of fire-resistant *P. sylvestris*, which reduced ecosystem
523 flammability by displacing more combustible taxa.

524 A synchronized surge since ~2 cal. kyr BP in charcoal influx occurred across
525 Regions A, B, C and D. This widespread intensification was driven by the synergistic
526 effects of regional climatic changes and intensified human activities (e.g., agricultural
527 expansion and pastoral burning), which overrode natural fuel limitations. Conversely,
528 Region G exhibited a marked decline in charcoal influx despite favorable climatic
529 conditions. This anomaly is attributed to landscape fragmentation caused by intensive
530 grazing, where livestock pressure reduced surface fuels and suppressed fire spread.

531 Our findings underscore that fire regimes in the Altai-Sayan ecoregion are
532 determined not just by climate, but by the specific flammability traits of dominant
533 vegetation (e.g., pyrophytic *Betula/Larix* vs. fire-resistant *P. sylvestris*) and land-use
534 history. Understanding these long-term fire-vegetation-human interactions provides
535 critical baselines for predicting future wildfire risks and implementing sustainable
536 forest management strategies in a warming world.

537

538 **CRedit authorship contribution statement**

539 Dongliang Zhang: Writing – review & editing, Validation, Methodology, Funding
540 acquisition, Conceptualization. Blyakharchuk Tatiana, Aizhi Sun, Xiaozhong Huang:
541 Writing – original draft, Visualization, Methodology, Data curation. Yuejing Li – Data
542 curation.

543 **Declaration of Competing Interest**

544 The authors declare that they have no known competing financial interests or personal
545 relationships that could have appeared to influence the work reported in this paper.

546 **Acknowledgment.** This research was financially supported by National Natural
547 Science Grants of China (No. 42471183), Youth Innovation Promotion Association of
548 Chinese Academy of Sciences (No. 2022447), National Natural Science Grants of
549 China (No. 42220104001) and Russian Budget project (No. FWRG-2026-0007). We
550 thank anonymous reviewers for their valuable comments, which significantly
551 improved the manuscript.

552 **References**

- 553 Agatova, A.R., Nepop, R.K., Bronnikova, M.A., Slyusarenko, I.Tu., Orlova, L.A.
554 Human occupation of South Eastern Altai highlands (Russia) in the context of
555 Environmental changes. *Archaeological and Anthropological Sciences*. DOI
556 10.1007/s12520-014-0202-7.
- 557 Aizen, E.M., Aizen, V.B., Melack, J.M., Nakamura, T., Ohta, T., 2001. Precipitation
558 and atmospheric circulation patterns at mid-latitudes of Asia. *Int. J. Climatol.* 21,
559 535-556.
- 560 Albrich, K., Rammer, W., Thom, D., Seidl, R., 2018. Trade-offs between temporal
561 stability and level of forest ecosystem services provisioning under climate
562 change. *Ecological Applications*, 28(7), 1884-1896.
- 563 Barhoumi, C., Bliedtner, M., Zech, R., Behling, H., 2024. Holocene vegetation, fire,
564 climate dynamics and human impact in the upper Orkhon Valley of the Khangai
565 Mountains, Mongolia. *Quat. Sci. Rev.* 334, 108713.
- 566 Blyakharchuk, T.A., Wright, H.E., Borodavko, P.S., van der Knaap, W.O., Ammann,
567 B., 2004. Late Glacial and Holocene vegetational changes on the Ulagan
568 high-mountain plateau, Altai Mountains, southern Siberia. *Palaeogeography*,

569 Palaeoclimatology, Palaeoecology, 209(1-4), 259-279.

570 Blyakharchuk, T.A., Wright, H.E., Borodavko, P.S., van der Knaap, W.O., Ammann,
571 B., 2007. Late glacial and Holocene vegetational history of the Altai mountains
572 (southwestern Tuva Republic, Siberia). *Palaeogeography, Palaeoclimatology,*
573 *Palaeoecology*, 245(3-4), 518-534.

574 Blyakharchuk, T.A., Wright, H.E., Borodavko, P.S., van der Knaap, W.O., Ammann,
575 B., 2008. The role of pingos in the development of the Dzhangyskol lake-pingo
576 complex, central Altai Mountains, southern Siberia. *Palaeogeography,*
577 *Palaeoclimatology, Palaeoecology*, 257(4), 404-420.

578 Blyakharchuk, T.A., Chernova, N.A., 2013. Vegetation and climate in the Western
579 Sayan Mts according to pollen data from Lugovoe Mire as a background for
580 prehistoric cultural change in southern Middle Siberia. *Quat. Sci. Rev.* 75, 22-42.

581 Blyakharchuk, T.A., Kuryina, I.V., Pologova, N.N., 2019. Late Holocene dynamics of
582 vegetation cover and climate humidity in the southeastern sector of the West
583 Siberian Plain according to palynological and rhizopod studies of peat deposits.
584 *Bulletin of Tomsk State University. Biology* 45, 164–189. (in Russian)

585 Blyakharchuk, T.A., Pupysheva, M.A., 2022. Indication of fires in the thousand-year
586 history of Central Altai. *Geography and Natural Resource*, 4, 128-136 (In
587 Russian).

588 Blyakharchuk, T.A., van Hardenbroek, M., Pupysheva, M.A., Kirpotin, S.N.,
589 Blyakharchuk, P.A., 2024. Late Glacial and Holocene history of climate,
590 vegetation landscapes and fires in South Taiga of Western Siberia based on
591 radiocarbon dating and multi-proxy palaeoecological research of sediments from
592 Shchuchye Lake. *Radiocarbon*, 1-24, doi:10.1017/RDC.2024.103.

593 Blyakharchuk, T.A., 2020. Dynamics of vegetation cover and quantitative
594 palaeoclimatic reconstructions in the Western Sayan Mountains from the Late
595 Glacial period to the present time according to a palynological study of the
596 Yuzhno-Buybinskoe mire. In *IOP Conference Series: Earth and Environmental*
597 *Science* (Vol. 611, No. 1, p. 012026). IOP Publishing.

598 Blaauw, M., Christen, J.A., 2011. Flexible paleoclimate age-depth models using an
599 autoregressive gamma process. *Bayesian Analysis* 6, 457–474.

600 Chen, X., 2010. *Geography of Chinese Arid Region*. Science Press, Beijing (in
601 Chinese).

602 Feng, Z.D., Sun, A.Z., Abdusalih, N., Ran, M., Kurban, A., Lan, B., Zhang, D.L.,
603 Yang, Y., 2017. Vegetation changes and associated climatic changes in the
604 southern Altai Mountains within China during the Holocene. *Holocene* 27 (5),
605 683-693.

606 Feurdean, A., Florescu, G., Tanțău, I., Vanni re, B., Diaconu, A. C., Pfeiffer, M.,
607 Kirpotin, S., 2020. Recent fire regime in the southern boreal forests of western
608 Siberia is unprecedented in the last five millennia. *Quat. Sci. Rev.* 244, 106495.

609 Feurdean, A., Diaconu, A.C., Pfeiffer, M., Gałka, M., Hutchinson, S.M., Butiseaca, G.,
610 Gorina, N., Tonlkov, S., Niamir, A., Tantau, I., Zhang, H., Kirpotin S., 2022.
611 Holocene wildfire regimes in Western Siberia: Interaction between peatland
612 moisture conditions and the composition of plant functional types. *Climate of the*
613 *Past* 18, 1255–1274

614 Fu, B.J., Liu, G.H., Ouyang, Z.Y., 2013. *Ecological regionalization in China*. Beijing:
615 Science Press.

616 Furyaev, V.V., 1996. *Role of Fire in Forest Development*. Nauka Publications:
617 Novosibirsk (In Russia).

618 Ivanova, G.A., Kukavskaya, E.A., Ivanov, V.A., Conard, S.G., McRae, D.J., 2020.
619 Fuel characteristics, loads and consumption in Scots pine forests of central
620 Siberia. *J. Forestry Res.* 31(6), 2507-2524.

621 Jones, M.W., Smith, A., Betts, R., Canadell, J.G., Prentice, I.C., Le Qu r , C., 2020.
622 Climate change increases the risk of wildfires. *ScienceBrief Rev.* 116, 117.

623 Kasischke, E.S., 2000. Boreal ecosystems in the global carbon cycle. In: Kasischke,
624 E.S., Stocks, B.J. (Eds.), *Fire, Climate Change, and Carbon Cycling in the Boreal*
625 *Forest*. Ecological.

626 Kharuk, V.I., Ponomarev, E.I., Ivanova, G.A., Dvinskaya, M.L., Coogan, S.C.,
627 Flannigan, M.D., 2021. Wildfires in the Siberian taiga. *Ambio*, 50(11),
628 1953-1974.

629 Kutzbach, J.E., Chen, G., Cheng, H., Edwards, R.L., Liu, Z., 2014. Potential role of
630 winter rainfall in explaining increased moisture in the Mediterranean and Middle
631 East during periods of maximum orbitally-forced insolation seasonality. *Clim.*
632 *Dyn.* 42 (3e4), 1079-1095.

633 Goldammer, J.G., Furyaev, V., 2013. Fire in ecosystems of boreal Eurasia (Vol. 48).
634 Springer Science & Business Media.

635 Hu, Y., Huang, X., Demberel, O., et al., 2024. Quantitative reconstruction of
636 precipitation changes in the Mongolian Altai Mountains since 13.7 ka. *Catena*,
637 234, 107536.

638 Hu, Y., Huang, X., Li, Y., et al., 2025. Holocene fire dynamics in the Altai Mountains
639 and its driving factors. *Geophysical Research Letters*, 52(9), e2025GL116309.

640 Li, Y., Zhang, Y., Wang, J., Wang, L., Li, Y., Chen, L., Zhao, L., Kong, Z., 2019.
641 Preliminary study on pollen, charcoal records and environmental evolution of
642 Alahake Saline Lake in Xinjiang since 4,700 cal yr BP. *Quat. Int.* 513, 8–17.

643 Li, Y., Zhang, D., Zhang, Y., Sun, A., Li, X., Huang, X., Zhang, Y., Li, Y., 2024.
644 Distentangling the late-Holocene human–environment interactions in the Altai
645 Mountains within the Arid Central Asia. *Palaeogeography, Palaeoclimatology,*
646 *Palaeoecology*, 654, 112466.

647 Liu, F., Liu, H., Xu, C., Shi, L., Zhu, X., Qi, Y., He, W., 2021. Old-growth forests
648 show low canopy resilience to droughts at the southern edge of the taiga. *Global*
649 *Change Biology*, 27(11), 2392-2402.

650 Marcott, S.A., Shakun, J.D., Clark, P.U., Mix, A.C., 2013. A reconstruction of
651 regional and global temperature for the past 11,300 years. *Science* 339,
652 1198-1201.

653 Mo, L., Zohner, C. M., Reich, P. B., Liang, J., De Miguel, S., Nabuurs, G. J., Ortiz-
654 Malavasi, E., 2023. Integrated global assessment of the natural forest carbon
655 potential. *Nature*, 624(7990), 92-101.

656 Panyushkina, I.P., 2012. Climate-Induced changes in Population Dynamics of
657 Siberian Scythians (700-250 B.C.). *Climate, Landscapes and Civilizations.*
658 *Geophysical Monograph Series* 198, 145-154.

659 Ponomarev, E.I., Kharuk, V.I., 2016. Wildfire occurrence in forests of the Altai-Sayan

660 region under current climate changes. *Contemporary Problems of Ecology*, 9,
661 29-36.

662 Power, M.J., Marlon, J., Ortiz, N., et al., 2007. Changes in fire regimes since the Last
663 Glacial Maximum: an assessment based on a global synthesis and analysis of
664 charcoal data. *Climate Dynamics*, 30, 887-907.

665 Reimer, P.J., Austin, W.E., Bard, E., Bayliss, A., Blackwell, P.G., Ramsey, C.B.,
666 Talamo, S., 2020. The IntCal20 Northern Hemisphere radiocarbon age
667 calibration curve (0–55 cal kBP). *Radiocarbon* 62 (4), 725–757.

668 Rudaya, N., Sergey, K., Michał, S., Xianyong, C., Snezhana, Z., 2020. Postglacial
669 history of the steppe Altai: climate, fire and plant diversity. *Quat. Sci. Rev.* 249,
670 106616.

671 Rudoy, A.N., Yatsuk, T.Yu., 1986. The palaeogeography of southeastern Altai.
672 *Chetvertichnaya geologiya i pervobytnaya arkheologiya*. Thesis of conference,
673 Ulan-Ude, 73–75.

674 Shi, C.M., Liang, Y., Gao, C., Wang, Q.H., Shu, L.F., 2020. Drought-modulated
675 boreal forest fire occurrence and linkage with La Nina events in Altai Mountains
676 Northwest China. *Atmosphere*, 11, 956.

677 Sun, A., Feng, Z.D., Ran, M., Zhang, C.J., 2013. Pollen-recorded bioclimatic
678 variations of the last ~22,600 years retrieved from Achit Nuur core in the western
679 Mongolian Plateau. *Quat. Int.* 311, 36-43.

680 Shi, C.M., Liang, Y., Gao, C., Wang, Q.H., Shu, L.F., 2020. Drought-modulated
681 boreal forest fire occurrence and linkage with La Nina events in Altai Mountains
682 Northwest China. *Atmosphere*, 11, 956.

683 Slavnin, V.D., Sherstova L.I. 1999. *Aerchaeologic-Ethnographic Essay of Northern*
684 *Khakassia in the Area of Geological Polygon of Siberian High School*). Tomsk
685 Polytechnical University Press, Tomsk (in Russian)

686 Tang, G., Yang, S., Miao, Y., et al., 2022. Grain size characteristics of microfossil
687 charcoal and the environmental implications in loess deposits from Ganzi,
688 Western Sichuan Plateau. *Journal of Lanzhou University (Natural Sciences)* 58
689 (03), 298–305 (in Chinese with English abstract).

690 Umbanhowar Jr, C.E., Shinneman, A.L., Tserenkhand, G., Hammon, E.R., Lor, P.,

691 Nail, K., 2009. Regional fire history based on charcoal analysis of sediments
692 from nine lakes in western Mongolia. *Holocene* 19(4), 611-624.

693 Unkelbach, J., Dulamsuren, C., Klinge, M., Behling, H., 2021. Holocene high-
694 resolution forest-steppe and environmental dynamics in the Tarvagatai
695 Mountains, northcentral Mongolia, over the last 9570 cal yr BP. *Quat. Sci. Rev.*
696 266, 107076.

697 Wang, W., Ma, Y.Z., Feng, Z.D., Narantsetseg, Ts, Liu, K.B., Zhai, X.W., 2011. A
698 prolonged dry mid-Holocene climate revealed by pollen and diatom records from
699 Lake Uggii Nuur in central Mongolia. *Quat. Int.* 229 (1e2), 74-83.

700 Wang, Z., Miao, Y., Zhao, Y., Zhang, Z., Zou, Y., Zhang, T., 2024. Preliminary
701 exploration of the fire activity recorded by microcharcoal in surface sediments of
702 Central and Western China. *Quat. Sci.* 44 (1), 201-213 (in Chinese with English
703 abstract).

704 Wood, S.N., 2017. *Generalized Additive Models: An Introduction with R* (2nd
705 Edition). Chapman and Hall/CRC, pp1-476.

706 Xiao, Y., Xiang, L., Huang, X., et al., 2021. Moisture changes in the Northern
707 Xinjiang Basin over the past 2400 years as Documented in Pollen Records of Jili
708 Lake. *Front. Earth Sci.* 9, 741992.

709 Xiang, L., Huang, X., Sun, M., Panizzo, V. N., Huang, C., Zheng, M., Chen, F., 2023.
710 Prehistoric population expansion in Central Asia promoted by the Altai Holocene
711 climatic optimum. *Nature Communications*, 14(1), 3102.

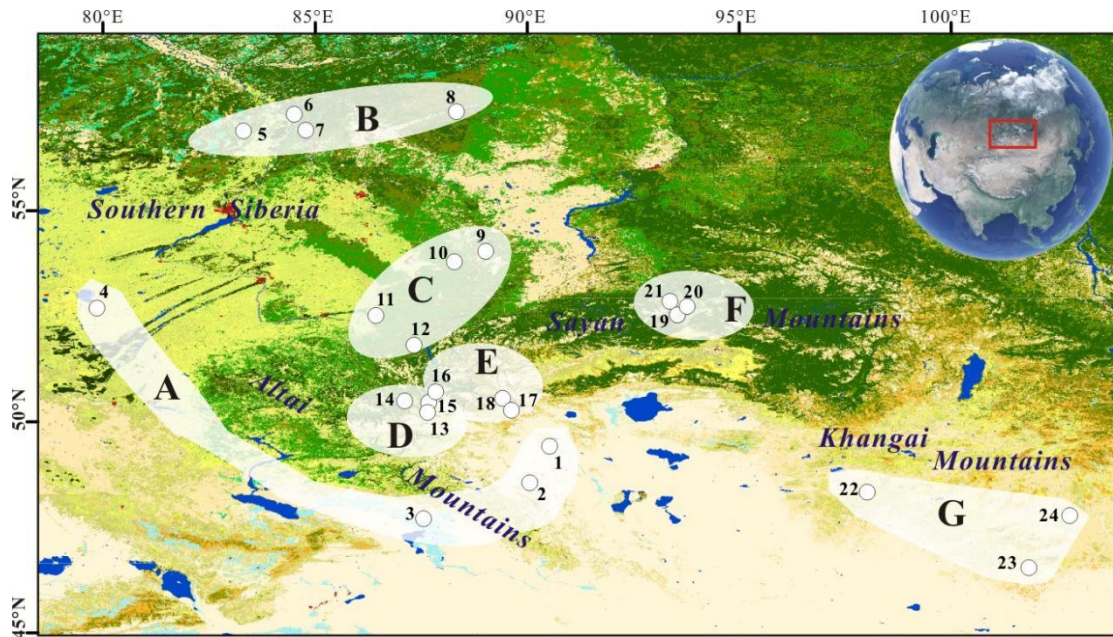
712 Xinjiang Comprehensive Expedition Team, Institute of Botany, Chinese Academy of
713 Sciences, 1978. *Vegetation and its utilization in Xinjiang*. Beijing: Science Press.

714 Zhang, D.L., Feng, Z.D., 2018. Holocene climate variations in the Altai Mountains
715 and the surrounding areas: a synthesis of pollen records. *Earth Sci. Rev.* 185,
716 847-869.

717 Zhang, D., Huang, X., Liu, Q., Chen, X., Feng, Z., 2022. Holocene fire records and
718 their drivers in the westerlies-dominated Central Asia. *Sci. Total Environ.* 833,
719 155153.

720 Zhang, D., Chen, X., Li, Y., Wang, W., Sun, A., Yang, Y., Feng, Z., 2020. Response of
721 vegetation to Holocene evolution of westerlies in the Asian Central Arid Zone.

722 Quaternary Science Reviews, 229, 106138.
723 Zhang, S.J., Lu, Y., Wei, W., Qiu, M., Dong, G., Liu, X., 2021. Human activities have
724 altered fire-climate relations in arid Central Asia since ~1000 a BP: evidence
725 from a 4200-year-old sedimentary archive. *Sci. Bull.* 66(8), 761-764.
726 Zhang, Y.Y., Zhang, D.L., 2025. Spatiotemporal patterns of pollen-based Holocene
727 precipitation variations in the Altai Mountains and the surrounding areas. *Global
728 and Planetary Change*, 251, 104832.
729 Zheng, B., Ciais, P., Chevallier, F., Yang, H., Canadell, J. G., Chen, Y., Zhang, Q.,
730 2023. Record-high CO₂ emissions from boreal fires in 2021. *Science*, 379(6635),
731 912-917.
732



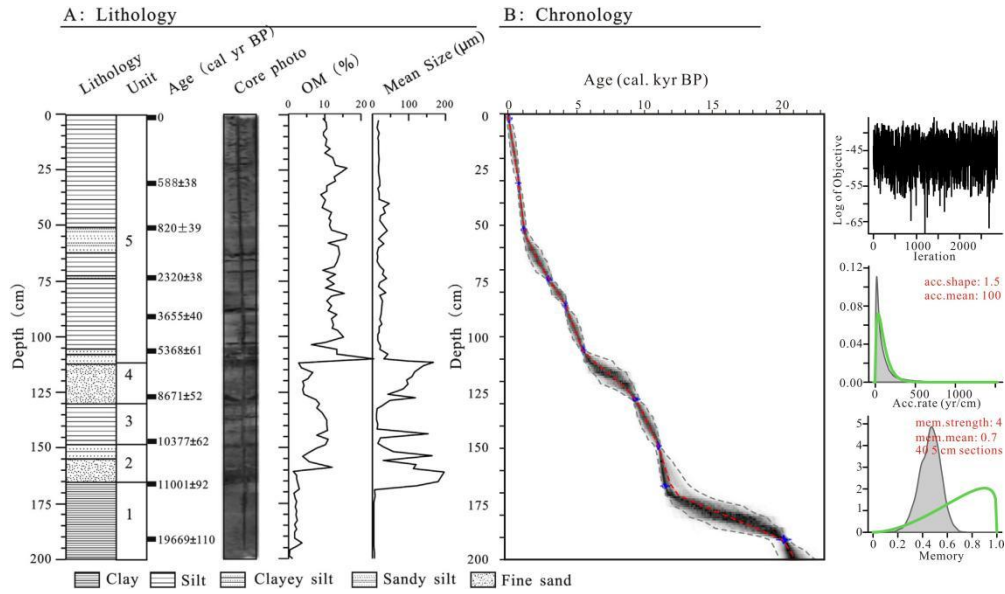
733

734 **Fig. 1.** Spatial distributions of the selected fossil pollen/charcoal sequences across the Altai- Sayan
 735 Mountains and adjacent plains. **Region A:** Achit Nuur (1), Tolbo Lake (2), Alahake Lake (3) and
 736 Kuchuk Lake (4); **Region B:** Rybnaya Mire (5), Plotnikovo Mire (6), Shchuchye Lake (7) and
 737 Ulukh–Chayakh Mire (8); **Region C:** Chudnoye Mire (9), Tundra Mire (10), Mokhovoe Bog (11)
 738 and Kuatang Mire (12); **Region D:** Dzhangyskol Lake (13), Uzunkol Lake (14) and Kendegelukol
 739 Lake (15); **Region E:** Tashkol Lake (16), Akkol Lake (17) and Grusha Lake (18); **Region F:**
 740 Buibinskoye Mire (19), Bezrybnoye Mire (20) and Lugovoe Peat (21); **Region G:** Olgi Lake (OL3)
 741 (22), Shireet Naiman Nuur (23) and Uggi Nuur (24).

742

743

744



745

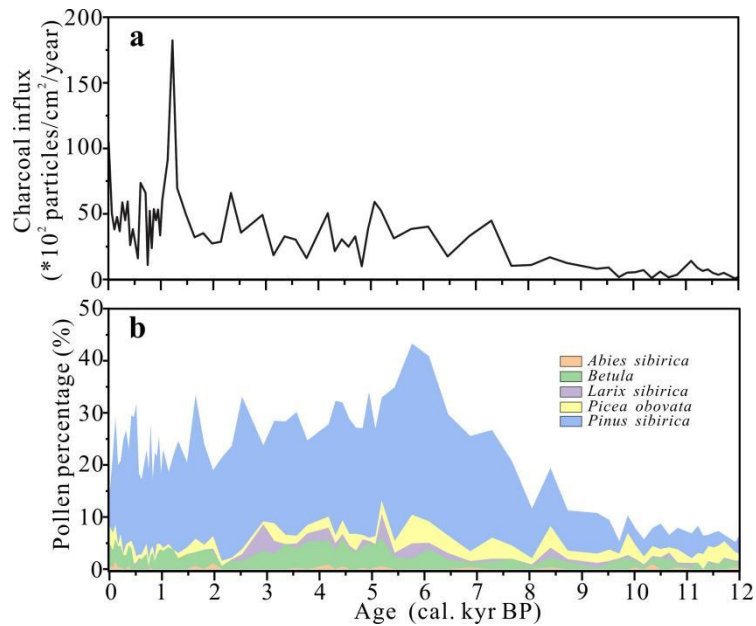
746 **Fig. 2.** Lithology, core photo, organic matter (OM), mean grain size and depth-age model in Achit

747

Nuur (modified from Sun et al., 2023).

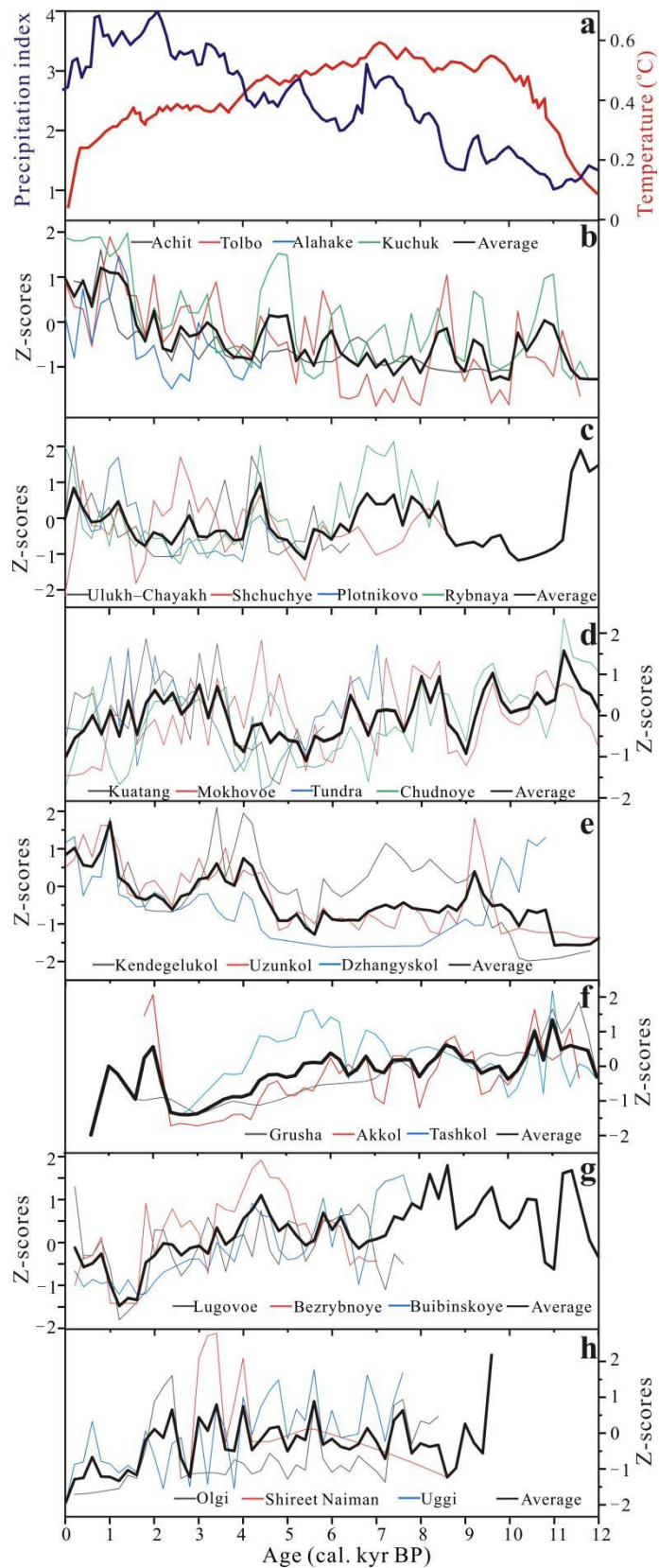
748

749



750

751 **Fig. 3.** Achit Nuur: charcoal influx (a) and vegetation change (b) (Sun et al., 2013; this study).



752

753 **Fig. 4.** Regional integrated charcoal influx (b-g) under the context of temperature (Marcott et al.,

754 2013) and precipitation index (a) in the Holocene interval (Zhang and Feng, 2018).

755

756 **Table 1** Detailed information of the selected sites around the Altai-Sayan Mountains and adjacent
 757 plains.

Region	No.	Site Name	Lat. (N)	Long. (E)	Elev. (m a.s.l.)	Core length (cm)	Time interval (cal. kyr BP)	type of charcoal	References
A	1	Achit Nuur	49.42	90.52	1444	200	22.6	micro	this study
	2	Tolbo Lake	48.55	90.05	2080	253	10.3	micro+macro	Hu et al., 2025
	3	Alahake Lake	47.69	87.54	483	140	4.7	micro	Li et al., 2021
	4	Kuchuk Lake	52.69	79.84	98	255	13.1	macro	Rudaya et al., 2020
B	5	Rybnaya Mire	57.28	84.49	-	400	8.4	macro	Feurdean et al., 2022
	6	Plotnikov o Mire	56.88	83.30	120	225	5	macro	Feurdean et al., 2020
	7	Shchuchye Lake	57.13	84.61	80	331	12.8	micro	Blyakharuk et al., 2024
	8	UluKh-Chayakh Mire	57.34	88.32	-	348	8.5	macro	Feurdean et al., 2022
C	9	Chudnoye Mire	54.03	89.01	1147	590	12.7	micro	Blyakharuk et al., 2024
	10	Tundra Mire	53.79	88.27	247	270	7.28	micro	Blyakharuk et al., 2024
	11	Mokhovoe Bog	52.52	86.42	283	638	16.19	micro	Blyakharuk, 2022
	12	Kuatang Mire	51.81	87.32	650	557	5.87	micro	Blyakharuk et al., 2024
D	13	Dzhangyskol Lake	50.18	87.73	1800	380	13	micro	Blyakharuk et al., 2008
	14	Uzunkol Lake	50.48	87.1	1985	285	12.02	micro	Blyakharuk et al., 2004
	15	Kendegelu kol Lake	50.50	87.63	2050	265	16.01	micro	Blyakharuk et al.,

									2004
	16	Tashkol Lake	50.45	87.67	2150	205	13.57	micro	Blyakhar huk et al., 2004
E	17	Akkol Lake	50.25	89.62	2204	470	14	micro	Blyakhar huk et al., 2007
	18	Grusha Lake	50.38	89.42	2413	241	14.37	micro	Blyakhar huk et al., 2007
	19	Buibinsko ye Mire	52.84	93.52	1377	600	13.11	micro	Blyakhar huk et al., 2022
F	20	Bezrybno ye Mire	52.81	93.50	1395	600	7.23	micro	Blyakhar huk et al., 2022
	21	Lugovoe Peat	52.85	93.35	1299	330	7.74	micro	Blyakhar huk et al., 2013
	22	Olgi Lake(OL3)	48.32	98.01	2012	235	9.57	micro	Unkelbac h et al., 2021
G	23	Shireet Naiman Nuur	46.53	101.82	2429	178	7.4	micro	Barhoumi et al., 2024
	24	Uggi Nuur	47.77	102.78	1330	200	22.6	micro	Wang et al., 2011

758

759

760

761 **Table 2** Correlation between the independent variables represented by pollen percentages (*Abies*,
762 *Betula*, *Larix*, *Picea*, *Pinus sibirica*, *Pinus sylvestris* and their sum (i.e., forest cover) and the
763 dependent variable (charcoal influx). The significance of each parameter is given by p values
764 where ***p < 0.001; **p < 0.01; *p < 0.05.

Site Name	Independent variable	edf	ref.df	F value	p-value	Deviance explained
Achit Nuur	<i>Abies</i>	-	-	-	-	-
	<i>Betula</i>	2.75	3.47	3.40	0.02*	21%
	<i>Larix</i>	3.51	4.21	8.72	0.00***	41.9%
	<i>Picea</i>	1	1	11.36	0.001**	19.2%
	<i>Pinus sibirica</i>	2.73	3.41	5.70	0.001**	34.5%
	<i>Pinus sylvestris</i>	-	-	-	-	-
	Forest cover	2.92	3.69	8.02	0.00***	41.5%
Tolbo Lake	<i>Abies</i>	-	-	-	-	-
	<i>Betula</i>	6.96	8.01	1.76	0.09	7.04%
	<i>Larix</i>	1.03	1.07	0.03	0.95	0.03%
	<i>Picea</i>	2.97	3.75	4.47	0.002**	8.11%
	<i>Pinus sibirica</i>	2.68	3.39	9.55	0.00***	13.3%
	<i>Pinus sylvestris</i>	-	-	-	-	-
	Forest cover	2.98	3.75	8.96	0.00***	14.3%
Alahake Lake	<i>Abies</i>	1	1	0.57	0.45	1.1%
	<i>Betula</i>	1	1	4.19	0.04*	5.2%
	<i>Larix</i>	6.85	7.94	1.42	0.19	11.6%
	<i>Picea</i>	3.84	4.77	1.96	0.09	10%
	<i>Pinus sibirica</i>	5.59	6.77	1.85	0.09	13%
	<i>Pinus sylvestris</i>	-	-	-	-	-
	Forest cover	2.17	2.77	1.24	0.26	5.07%
Kuchuk Lake	<i>Abies</i>	1.21	1.40	3.80	0.03*	9.81%
	<i>Betula</i>	1.38	1.67	16.18	0.00***	25.2%
	<i>Larix</i>	1.11	1.21	0.01	0.98	0.19%
	<i>Picea</i>	1.16	1.30	1.31	0.30	2.29%
	<i>Pinus sibirica</i>	5.84	6.89	1.06	0.39	9.51%
	<i>Pinus sylvestris</i>	6.54	7.64	2.61	0.01*	25.5%
	Forest cover	3.59	4.47	1.22	0.28	11%
Rybnaya Mire	<i>Abies</i>	5.28	6.31	1.99	0.07	11.7%
	<i>Betula</i>	4.90	6.00	3.32	0.004**	18.4%
	<i>Larix</i>	7.07	8.11	1.95	0.07	20.6%
	<i>Picea</i>	8.15	8.79	14.1	0.00***	44.5%
	<i>Pinus sibirica</i>	6.74	7.86	1.68	0.12	16.6%
	<i>Pinus sylvestris</i>	2.03	2.54	1.06	0.35	4%
	Forest cover	7.00	8.10	3.06	0.003**	16.2%
Plotnikovo	<i>Abies</i>	3.12	3.88	0.70	0.55	16.7%

Mire	<i>Betula</i>	2.69	3.36	1.40	0.26	19.6%	
	<i>Larix</i>	1	1	4.09	0.06	20.1%	
	<i>Picea</i>	2.12	2.65	1.54	0.26	15.1%	
	<i>Pinus sibirica</i>	1.68	2.11	0.41	0.7	4.85%	
	<i>Pinus sylvestris</i>	2.01	2.53	1.50	0.23	14.7%	
	Forest cover	4.43	5.21	4.07	0.004**	39.7%	
Schuchye Lake	<i>Abies</i>	4.78	5.85	5.39	0.00***	37.4%	
	<i>Betula</i>	1	1	5.29	0.03*	10.8%	
	<i>Larix</i>	1	1	63.71	0.00***	45.4%	
	<i>Picea</i>	2.19	2.71	3.77	0.02*	17.5%	
	<i>Pinus sibirica</i>	1	1	27.6	0.00***	30.8%	
	<i>Pinus sylvestris</i>	3.15	3.90	3.31	0.02*	21.2%	
	Forest cover	2.10	2.52	7.91	0.00***	24.7%	
Ulukh–Chay akh Mire	<i>Abies</i>	6.38	7.52	1.60	0.18	29.4%	
	<i>Betula</i>	1	1	6.44	0.01*	13.4%	
	<i>Larix</i>	2.54	3.16	2.46	0.07	17.5%	
	<i>Picea</i>	2.45	3.12	1.46	0.23	16.7%	
	<i>Pinus sibirica</i>	1	1	0.66	0.42	1.82%	
	<i>Pinus sylvestris</i>	1	1	4.43	0.04*	10.3%	
Forest cover		4.26	5.08	1.46	0.22	16.9%	
	Chudnoye Lake	<i>Abies</i>	1.75	2.17	2.09	0.14	8.52%
		<i>Betula</i>	1.23	1.42	10.54	0.001**	23.5%
		<i>Larix</i>	2.06	2.57	3.84	0.03*	14.7%
		<i>Picea</i>	1.99	2.44	11.76	0.00***	30.3%
		<i>Pinus sibirica</i>	4.33	5.25	3.38	0.01*	26.6%
<i>Pinus sylvestris</i>		1	1	6.59	0.01*	11.6%	
Forest cover		1	1	1.97	0.17	3.5%	
Tundra Mire	<i>Abies</i>	2.16	2.75	0.78	0.57	3.83%	
	<i>Betula</i>	1	1	3.27	0.07	4.44%	
	<i>Larix</i>	6.41	7.35	4.32	0.00***	22.7%	
	<i>Picea</i>	1	1	0.09	0.77	0.13%	
	<i>Pinus sibirica</i>	2.39	2.99	0.83	0.46	4.66%	
	<i>Pinus sylvestris</i>	3.03	3.78	0.79	0.49	5.83%	
Forest cover		1	1	2.79	0.10	3.53%	
	Mokhove Bog	<i>Abies</i>	1.83	2.31	1.12	0.38	3.65%
		<i>Betula</i>	6.81	7.88	2.07	0.05	17.2%
		<i>Larix</i>	1.09	1.17	0.24	0.63	0.59%
		<i>Picea</i>	2.59	3.22	3.54	0.02*	11.9%
		<i>Pinus sibirica</i>	1	1	0.00	0.96	0.003%
<i>Pinus sylvestris</i>		4.46	5.49	1.78	0.11	13%	
Forest cover		5.04	6.19	0.91	0.48	10.3%	
	Kuatang Mire	<i>Abies</i>	2.45	3.14	2.78	0.04*	13.8%
<i>Betula</i>		1	1	29.13	0.00***	24.5%	

	<i>Larix</i>	1	1.00	0.06	0.81	0.08%
	<i>Picea</i>	6.72	7.79	1.19	0.31	13.4%
	<i>Pinus sibirica</i>	1.43	1.74	2.92	0.05*	6.90%
	<i>Pinus sylvestris</i>	1	1	5.83	0.02*	6.51%
	Forest cover	1	1	9.24	0.003**	10.9%
Dzhangyskol Lake	<i>Abies</i>	3.64	4.53	0.45	0.79	16.9%
	<i>Betula</i>	1.79	2.23	0.37	0.77	7.12%
	<i>Larix</i>	1	1	0.05	0.83	0.33%
	<i>Picea</i>	3.92	4.80	0.82	0.51	24.8%
	<i>Pinus sibirica</i>	1.70	2.12	0.35	0.73	7.06%
	<i>Pinus sylvestris</i>	3.05	3.75	1.22	0.29	22.8%
	Forest cover	2.39	3.04	0.67	0.58	15.6%
Uzunkol Lake	<i>Abies</i>	1	1	5.329	0.02*	7.04%
	<i>Betula</i>	4.92	5.99	3.22	0.01**	29.4%
	<i>Larix</i>	1	1	14.38	0.00***	22.1%
	<i>Picea</i>	5.99	7.12	5.03	0.00***	40.1%
	<i>Pinus sibirica</i>	2.04	2.57	1.99	0.14	14.7%
	<i>Pinus sylvestris</i>	4.79	5.81	2.85	0.02*	29.3%
	Forest cover	2.17	2.69	1.39	0.27	14.2%
Kendegeluko Lake	<i>Abies</i>	4.93	5.97	2.63	0.04*	41.4%
	<i>Betula</i>	5.87	7.04	2.78	0.02*	49.4%
	<i>Larix</i>	1	1	3.11	0.09	9.63%
	<i>Picea</i>	2.99	3.73	2.19	0.08	29.4%
	<i>Pinus sibirica</i>	2.25	2.78	2.26	0.09	28.9%
	<i>Pinus sylvestris</i>	1	1	18.48	0.00***	40%
	Forest cover	1.57	1.91	3.58	0.06	26.9%
Tashkol Lake	<i>Abies</i>	1	1	0.02	0.90	0.09%
	<i>Betula</i>	1	1	0.08	0.79	0.36%
	<i>Larix</i>	1.56	1.92	0.20	0.82	3.52%
	<i>Picea</i>	6.69	7.81	2.35	0.04*	40.7%
	<i>Pinus sibirica</i>	1	1	0.004	0.95	0.02%
	<i>Pinus sylvestris</i>	1	1	0.02	0.89	0.09%
	Forest cover	3.00	3.75	0.90	0.48	17%
Akkol Lake	<i>Abies</i>	1.76	2.11	0.79	0.43	4.83%
	<i>Betula</i>	1	1	0.96	0.33	1.76%
	<i>Larix</i>	6.53	7.59	1.94	0.08	30.4%
	<i>Picea</i>	2.41	3.03	6.77	0.00***	31.6%
	<i>Pinus sibirica</i>	4.35	5.41	1.90	0.1	23%
	<i>Pinus sylvestris</i>	1	1	10.12	0.002**	18.9%
	Forest cover	8.47	8.92	5.49	0.00***	55.1%
Grusha Lake	<i>Abies</i>	1	1	0.62	0.44	2.75%
	<i>Betula</i>	1	1	0.88	0.36	3.93%

	<i>Larix</i>	3.81	4.58	3.44	0.02*	49.3%
	<i>Picea</i>	2.18	2.71	3.30	0.05*	35.80%
	<i>Pinus sibirica</i>	1	1	0.60	0.45	2.67%
	<i>Pinus sylvestris</i>	1.39	1.66	0.19	0.76	4.67%
	Forest cover	2.55	3.18	12.7	0.00***	71.1%
Bezrybnoe Mire	<i>Abies</i>	1.15	1.29	0.31	0.75	1.16%
	<i>Betula</i>	1.74	2.20	1.63	0.22	8.85%
	<i>Larix</i>	2.58	3.14	0.32	0.79	4.76%
	<i>Picea</i>	1	1	2.13	0.15	4.49%
	<i>Pinus sibirica</i>	1.37	1.66	0.39	0.75	2.18%
	<i>Pinus sylvestris</i>	6.47	7.53	1.69	0.13	28.1%
	Forest cover	1	1	0.01	0.93	0.02%
Buibinskoye Mire	<i>Abies</i>	2.71	3.39	4.85	0.004**	29.6%
	<i>Betula</i>	2.11	2.69	2.29	0.10	17.4%
	<i>Larix</i>	1	1	1.16	0.29	2.83%
	<i>Picea</i>	1.52	1.87	0.71	0.40	4.85%
	<i>Pinus sibirica</i>	2.02	2.57	2.70	0.05	17.4%
	<i>Pinus sylvestris</i>	1	1	3.78	0.06	7.42%
	Forest cover	3.61	4.42	2.47	0.06	22.6%
Lugovoe Mire	<i>Abies</i>	1	1	6.32	0.02*	15.3%
	<i>Betula</i>	1	1	0.23	0.64	0.79%
	<i>Larix</i>	5.00	5.91	3.89	0.01**	43.5%
	<i>Picea</i>	4.00	4.95	2.41	0.07	35.8%
	<i>Pinus sibirica</i>	3.43	4.28	2.20	0.09	31%
	<i>Pinus sylvestris</i>	8.81	8.98	3.21	0.01*	60.5%
	Forest cover	1.14	1.27	0.20	0.67	2.29%
Olgi Lake	<i>Abies</i>	-	-	-	-	-
	<i>Betula</i>	4.89	5.96	2.91	0.02*	34.5%
	<i>Larix</i>	4.32	5.29	2.68	0.03*	35.6%
	<i>Picea</i>	3.8	4.65	4.20	0.003**	35.7%
	<i>Pinus sibirica</i>	8.62	8.89	45.23	0.00***	27.9%
	<i>Pinus sylvestris</i>	-	-	-	-	-
	Forest cover	1.74	2.21	7.46	0.00***	33.3%
Shireet Naiman Nuur	<i>Abies</i>	-	-	-	-	-
	<i>Betula</i>	2.57	3.211	3.82	0.01*	20.7%
	<i>Larix</i>	1	1	1.59	0.21	2.83%
	<i>Picea</i>	1	1	6.55	0.01*	9.70%
	<i>Pinus sibirica</i>	3.98	4.91	4.02	0.003**	27.5%
	<i>Pinus sylvestris</i>	1	1	7.99	0.01**	12%
	Forest cover	4.01	4.96	6.38	0.00***	37.4%
Uggi Nuur	<i>Abies</i>	-	-	-	-	-
	<i>Betula</i>	6.49	7.59	2.02	0.06	8.65%
	<i>Larix</i>	6.48	0.06	104.4	0.00***	12.2%

<i>Picea</i>	1	1	0.18	0.67	0.1%
<i>Pinus sibirica</i>	8.55	8.94	6.19	0.00***	19.4%
<i>Pinus sylvestris</i>	-	-	-	-	-
Forest cover	8.07	8.76	5.72	0.00***	18.4%

765

766